Asia-Pacific Journal of Science and Technology :Volume :26 .Issue .02 :Article ID :.APST-26-02-13. Research Article

APST

Asia-Pacific Journal of Science and Technology

https//:www.tci-thaijo.org/index.php/APST/index

Published by the Research and Graduate Studies,
Khon Kaen University, Thailand

Simple soft chemical synthesis and characterization of phase pure co-doped $LiMn_2O_4$ nanoparticles as cathode materials for Li-ion battery applications

Alagu S. Deepi[1], Gopalakrishnan Srikesh[1] and Arputharaj S. Nesaraj[1,*],

[1]Department of Applied Chemistry, Karunya Institute of Technology and Sciences (Deemed to be University), Tamil Nadu, India
[*]Corresponding author: drsamson@karunya.edu

Received 3 January 2020
Revised 10 March 2021
Accepted 16 March 2021

Abstract

Spinel $LiMn_2O_4$ is considered as a best cathode material for Li-battery applications. Lithium ion battery has high energy density and long service life and hence it is used in portable electronic devices and electric vehicles. In this research work, a series of Co-doped $LiMn_2O_4$ nanoparticles, viz. $LiMn_{2-x}Co_xO_{4-\delta}$ (where x = 0, 0.1, 0.2, 0.3, 0.4 and 0.5) were prepared by a simple one-pot combustion synthetic route with urea as an organic fuel. The prepared materials were characterized by X-ray Diffraction (XRD), Fourier Transform Infrared Spectroscopy (FTIR), particle size analysis, Scanning Electron Microscope (SEM) and Energy Dispersive X-ray (EDAX) analysis. The electrochemical properties of the prepared materials were studied by AC impedance analysis. The result indicates that doping of Co in $LiMn_2O_4$ can improve the electrical characteristics of the spinel. It was found that $LiMn_{1.5}Co_{0.5}O_{4-\delta}$ sintered specimen has shown better conductivity value of 1.45 x 10^{-5} Scm^{-1} among all other samples studied. Based on the results, we propose that Co-doped $LiMn_2O_4$ spinel can be an attractive cathode material for Li-ion battery applications.

Keywords: Li-ion battery, Alternate cathode, Combustion synthesis, Characterization

1. Introduction

Li-ion batteries are found applications in electronic gadgets, viz., cell phones, cameras, wall clocks, mini computers, electric vehicles, etc. because of their large terminal voltage and a large energy density [1]. In practice, the cathode material plays a major part in finding the efficiency of the lithium ion battery. Hence, loads of efforts have been taken in bringing forth the high density material with low cost and good cycling stability [2,32]. Earlier, $LiCoO_2$ was practically used as cathode component in lithium ion batteries. On considering its disadvantages like high cost, toxicity and security purposes various attempts were taken for alternative cathode material like $LiMn_2O_4$, $LiFePO_4$, $LiAlO_2$, $LiNiO_2$ and few more [3-4,31]. $LiMn_2O_4$ spinel is a widely used cathode material for Li-ion rechargeable batteries because it has many advantages, such as plentiful manganese resources, less toxicity, low cost and environmental friendliness compared to other $LiCoO_2$ and $LiNiO_2$ [5]. The theoretical specific capacitance of $LiMn_2O_4$ is 148 mAh g-1 [33] which has some critical deficiency such as $LiMn_2O_4$ experiences rigorous capacity fading, especially at high temperature (55 $^{\circ}$C) during discharging/charging [6].

There are few supporting reasons for their poor electrochemical performance for $LiMn_2O_4$. Some of the reasons are as follows.

1. According to Jahn-Teller effect, there will be blockage in transporting Li+ ions due to the damage in structure during the transition of spinel $LiMn_2O_4$ from cubic phase to tetragonal phase [7].
2. The existence of huge amount of Mn^{4+} and high charge-voltage plateau even after complete charging would fasten up the decomposition of electrolyte [8].
3. The unbalanced reaction between the Mn^{3+} present the particle surface and the soluble Mn^{3+} available in the electrolyte results in the increase of cell impedance and lowering of active Mn^{3+}. The researchers have made

several attempts to synthesize modified $LiMn_2O_4$ doped with various metal ions such as, Al [9], Ni [10], Mg [11], Fe [12], Zn [13], etc. especially to slow down capacity fading and to increase the electrochemical characteristics. Among the dopant material used cobalt is considered to be one of the best to solve the technological problems. Because of the smaller radius of Co^{3+} it tends to enhance the valence of manganese ions and enhance the strength of M-O bonding in the $LiMn_2O_4$ lattice and also increase the cycle performance of the spinel $LiMn_2O_4$. In the doped materials, Co is suitable for doping materials based on the ionic radius which is smaller than the Mn^{3+} and the Co-O bond is much stronger than the any other metal oxygen bonding [14]. Thus, this Co-doped cathode materials can exhibit significantly improved conductivity when compared with undoped $LiMn_2O_4$. It was found that the electrochemical behavior of $LiMn_2O_4$ is strongly influenced by the preparation procedures. Many methodologies, such as solid state process [15], sono-chemical reaction [16], chemical precipitation [17], sol-gel synthesis [18], combustion route [19], etc. In this paper, we describe a simple one pot combustion synthesis [19] of Co-doped $LiMn_2O_4$ nanoparticles and their physico-chemical / electro-chemical characterization for use as the cathode material in lithium-ion based electrochemical devices.

2. Materials and methods

2.1 Preparation and physical characterization of cobalt doped $LiMn_2O_4$ nanoparticles

In this research work, Co-doped $LiMn_2O_4$ nanoparticles, viz. $LiMn_{2-x}Co_xO_{4-\delta}$ (where x = 0, 0.1, 0.2, 0.3, 0.4 and 0.5) were prepared by a simple one pot combustion process with urea as an organic fuel [20]. The following chemical reagents were used in the synthesis. Cobalt nitrate (98%, Lobachemie, India), lithium nitrate (98%, Merck, India) and manganese nitrate (98%, Merck, India) were used as precursor salts and urea (99.5%, Merck, India) as a fuel. All the chemical reagents were analytically pure and used without any further purification. According to propellant chemistry calculations, the species, Li^+, Mn^{2+}, Co^{2+}, carbon and hydrogen are reducing species with corresponding valencies +1, +2, +2, +4 and +1. Elemental oxygen is an oxidizing agent with valency +2. The valency of nitrogen is zero [20]. Based on this contemplation, lithium nitrate, manganese nitrate and cobalt nitrate will have the oxidizing valencies of -5, -10 and -10 respectively. The urea fuel has the reducing valency of +6.

In a typical experiment, appropriate quantities of lithium nitrate [$LiNO_3$], manganese nitrate [$Mn(NO_3)_2.4H_2O$], cobalt nitrate [$Co(NO_3)_2.6H_2O$] and urea were dissolved in distilled water taken in a silica crucible. The solution was heated until the volume of the solution was reduced to half. The crucible containing the solution was kept in to a muffle furnace at 600 $^{\circ}$C where it boiled, frothed, ignited and resulted in fire (temperature could rise up to 1100 ± 100 $^{\circ}$C). At this temperature, the metal nitrate salts decomposed to metal oxides and nitrogen which led to the formation of foamy combustion material in less than 5 minutes. The flame remained for about 1 minute. The foam was crushed well in a glass mortar get fine nanoparticles. It was reported that during flaming reaction, the temperature is raised above 1000 $^{\circ}$C. The gases formed during the reaction not only yield very small particles of $LiMn_{2-x}Co_xO_{4-\delta}$ but also help to drive away the heat which restricts the sintering of the product [20]. The stoichiometric redox reactions between nitrate salt precursors and urea fuel to produce $LiMn_{2-x}Co_xO_{4-\delta}$ (where x = 0, 0.1, 0.2, 0.3, 0.4 and 0.5) nanoparticles can be shown by a following common theoretical equation (1)

$$LiNO_3 + (2\text{-}x)\ Mn(NO_3)_2 + x\ Co(NO_3)_2 + 4.165\ NH_2CONH_2 \rightarrow LiMn_{2-x}Co_xO_{4-\delta} + 6.665\ N_2 + 4.165\ CO_2 + 8.33\ H_2O \quad (1)$$

The powder XRD study was done by a Shimadzu XRD6000 X-ray diffractometer at a scan speed of 5 deg/min with CuKα radiation. The crystallite sizes of the particles were calculated by Scherrer's formula. FTIR spectra of all the samples were studied by Shimadzu IR Prestige-21 model FTIR spectrometer. The particle characteristics the powder was checked using Malvern particle size analyzer (Malvern Instruments, Worcestershire, UK) with water as medium. The morphology of the oxide was studied by JEOL Model JSM-6360 scanning electron microscope and the atomic weight percentage of the elements present was measured by Energy dispersive X-ray (EDAX) using the same instrument.

2.2 Fabrication of $LiMn_{2-x}Co_xO_{4-\delta}$ spinel electrodes and their electrochemical characterization

The resultant $LiMn_{2-x}Co_xO_{4-\delta}$ spinel powder was mixed well with the addition of few drops of PVA (poly vinyl alcohol) binder solution and placed in a die. The circular cathode discs were compacted at 4000 kg/cm^2 pressure with a hydraulic machine. The thickness of the compacts was found to be in the range of 1.8-2.4 cm with a diameter of 1 cm. The pellets were sintered at 600 $^{\circ}$C for 6 in air before subjecting them to electrochemical measurements. The electrochemical impedance studies were conducted using an electrochemical work station with two electrode system under aluminium foil substrate in the frequency

between 40 Hz - 1 MHz at 27 °C. The counter electrode is aluminium foil. Data acquisition and analysis are done, respectively, using the electrochemical impedance software.

3. Results and discussion

3.1 XRD studies

Figure 1 exhibits the XRD pattern obtained on the pure $LiMn_2O_4$ and Co-doped $LiMn_2O_4$ nanoparticles synthesized by combustion technique with urea as an organic fuel.

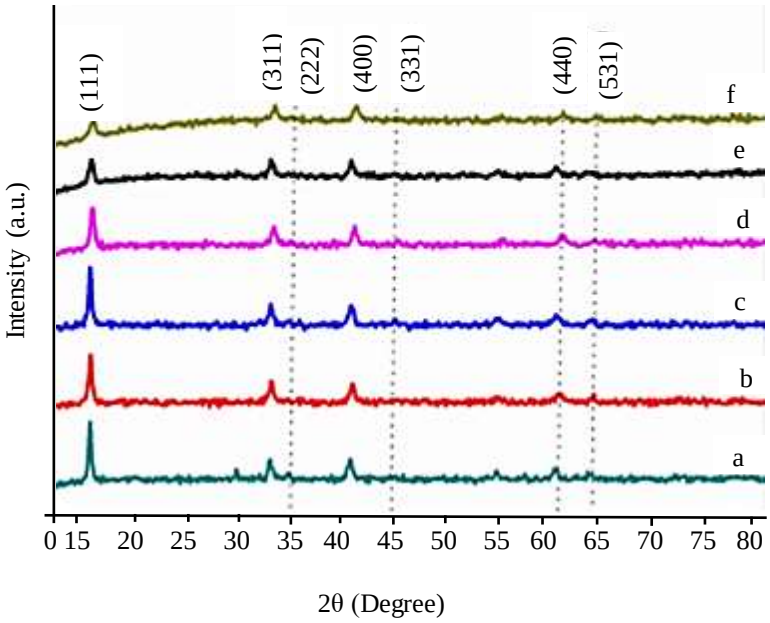

Figure 1 XRD patterns got on parent $LiMn_2O_4$ and Co-doped $LiMn_2O_4$ such as (a) pure $LiMn_2O_4$, (b) $LiMn_{1.9}Co_{0.1}O_{4-\delta}$, (c) $LiMn_{1.8}Co_{0.2}O_{4-\delta}$, (d) $LiMn_{1.7}Co_{0.3}O_{4-\delta}$, (e) $LiMn_{1.6}Co_{0.4}O_{4-\delta}$, (f) $LiMn_{1.5}Co_{0.5}O_{4-\delta}$ nanoparticles prepared by combustion technique.

It clearly shows several sharp diffraction peaks for all the samples. The resulted sharp peaks in the XRD diagrams exhibit the crystalline nature of the particles because of high temperature calcination done at 600° C. The XRD patterns of $LiMn_2O_4$ and doped $LiMn_2O_4$ were matched with the reported JCPDS data for $LiMn_2O_4$ (JCPDS card No: 89-8325). The XRD patterns of calcined Co-doped $LiMn_2O_4$ reveal the presence of well-crystallized cubic geometry as reported [21]. No other peaks were observed which illustrates the complete formation of $LiMn_2O_4$. As seen in the figure no peak shift observed, this indicated that the Co^{3+} has been completely into the bulk structure of $LiMn_2O_4$ rather than just doping on the surface [22].The lattice parameters were calculated from 2θ peaks in the X-ray diffraction pattern. From the data, it was found that the unit cell parameter reduces with enhancement in the concentration of cobalt dopant. This may be due to the formation of Mn^{3+} and Mn^{4+} in the $LiMn_{2-x}Co_xO_{4-\delta}$ nanoparticles [23]. Also, the decrease in lattice constant of $LiMn_{2-x}Co_xO_{4-\delta}$ with increase in the concentration of cobalt may also be endorsed to the elevated local strain induced by greater amount cobalt doping [24]. The crystallite sizes have been measured by Scherrer's equation(2). The crystallographic data obtained on Co-doped $LiMn_2O_4$ nanoparticles are indicated in Table 1.

$$D = \frac{k\lambda}{\beta \cos\theta} \qquad (2)$$

where 'D' is the crystalllite size, 'k' is the numerical constant (~0.9), 'λ' is the wavelength of x-rays (for CuKα radiation, λ = 1.5418 Å), 'β' is the effective broadening taken as a full width at half maximum (FWHM) (in radians), 'θ' is the diffraction angle for the peak. The crystallite size of the materials, determined with Scherrer's formula, was reported to be 8.9 to 22 nm. The crystallite size for $LiMn_2O_4$ samples was reported to be 20 – 27 nm prepared by solution combustion method [25].

Table 1 Crystallographic data obtained on $LiMn_{2-x}Co_xO_{4-\delta}$ nanoparticles.

Material	Crystalline structure	Unit cell parameter 'a' (Å)	Unit cell volume (Å^3)	2θ	β	Crystallite size (nm)
$LiMn_2O_4$	Cubic spinel	8.119	535.18	18.9150	0.77730	10.6
$LiMn_{1.9}Co_{0.1}O_{4-\delta}$	Cubic spinel	8.169	545.13	18.8185	0.36100	22.8
$LiMn_{1.8}Co_{0.2}O_{4-\delta}$	Cubic spinel	8.160	544.33	18.7985	0.44880	18.4
$LiMn_{1.7}Co_{0.3}O_{4-\delta}$	Cubic spinel	8.152	541.74	18.8381	0.47510	17.3
$LiMn_{1.6}Co_{0.4}O_{4-\delta}$	Cubic spinel	8.068	525.16	19.0352	0.53520	15.5
$LiMn_{1.5}Co_{0.5}O_{4-\delta}$	Cubic spinel	8.062	523.99	19.0492	0.91980	8.9

3.2 FTIR studies

In order to discover the functional groups present in the as prepared materials, FTIR spectra of the $LiMn_{2-x}Co_xO_{4-\delta}$ nanoparticles were studied at room temperature. Figure 2 exhibits the FTIR spectra obtained on the pure $LiMn_2O_4$ and Co-doped $LiMn_2O_4$ nanoparticles synthesized by combustion route with urea as organic fuel. The peaks appeared at 515.98 - 636.54 cm^{-1} in all the samples of pure $LiMn_2O_4$, $LiMn_{1.9}Co_{0.1}O_{4-\delta}$, $LiMn_{1.8}Co_{0.2}O_{4-\delta}$, $LiMn_{1.7}Co_{0.3}O_{4-\delta}$, $LiMn_{1.6}Co_{0.4}O_{4-\delta}$ and $LiMn_{1.5}Co_{0.5}O_{4-\delta}$ may be attributed to metal - oxygen vibrations (Li-O, Mn-O) in the prepared samples. The presence of metal-oxygen bond was also confirmed by the peaks appeared below 1500 cm^{-1} in the powder materials [26]. A broad absorption band appeared near 3,000 cm^{-1}, is indexed for O–H stretching vibration in the samples [27].

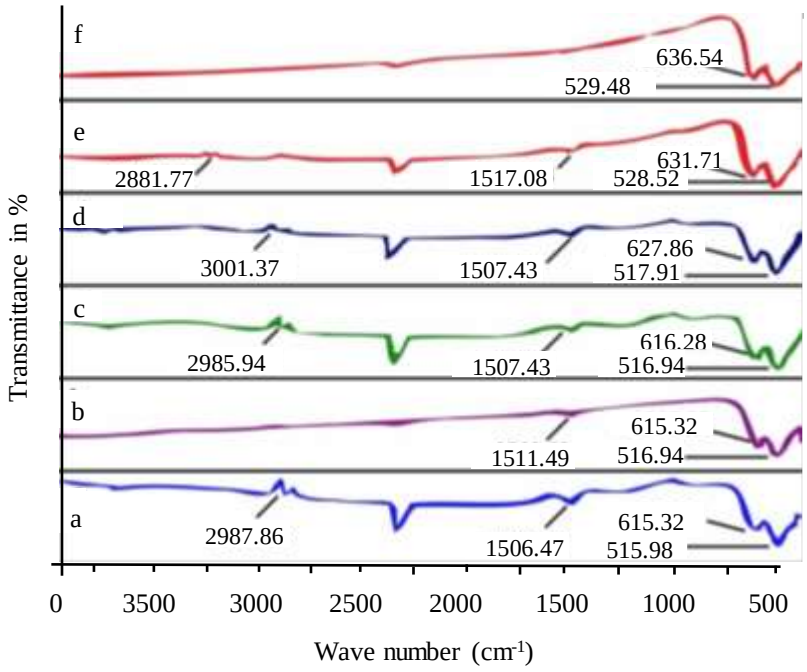

Figure 2 FTIR spectra obtained on parent $LiMn_2O_4$ and Co-doped $LiMn_2O_4$ such as (a) pure $LiMn_2O_4$, (b) $LiMn_{1.9}Co_{0.1}O_{4-\delta}$, (c) $LiMn_{1.8}Co_{0.2}O_{4-\delta}$, (d) $LiMn_{1.7}Co_{0.3}O_{4-\delta}$, (e) $LiMn_{1.6}Co_{0.4}O_{4-\delta}$, (f) $LiMn_{1.5}Co_{0.5}O_{4-\delta}$ nanoparticles prepared by combustion technique.

From this, it was understood that the ultrapure smaller particles may tend to physically suck up atmospheric water molecules. The peaks emerged at 1500-1520 cm^{-1} may be due to Li-O bending vibration modes in the samples [28]. The peaks appeared at 2400 cm^{-1} may be due to the presence of CO_2 in the sample [29].

3.3 Particle size analysis

The particle size diagrams of the Co-doped $LiMn_2O_4$ nanoparticles synthesized by combustion method are shown in Figure 3. In all the measurements, about 0.01 g of material was sonicated in 10 mL of double distilled water for about 20 minutes before subjecting the samples for particle size analysis. The resulted data is presented in Table 2. From the particle size characteristics (Table 2), it was understood that the particle size of the doped materials is less when compared with the parent $LiMn_2O_4$. The particle characteristics of the samples are found to be in the range of 196.6-294.9 nm. The presence of larger particles could be due to the agglomeration of smaller particles at high temperature heat treatment process [30]. The agglomeration found in $LiMn_{2-x}Co_xO_{4-\delta}$ particles was mainly due to the high temperature calcinations process [20]. Also, it was found that due to their large surface-to-volume ratio, $LiMn_{2-x}Co_xO_{4-\delta}$ particles have high surface energies and therefore tend to agglomerate and form clusters thus resulting in enhanced particle size [31].

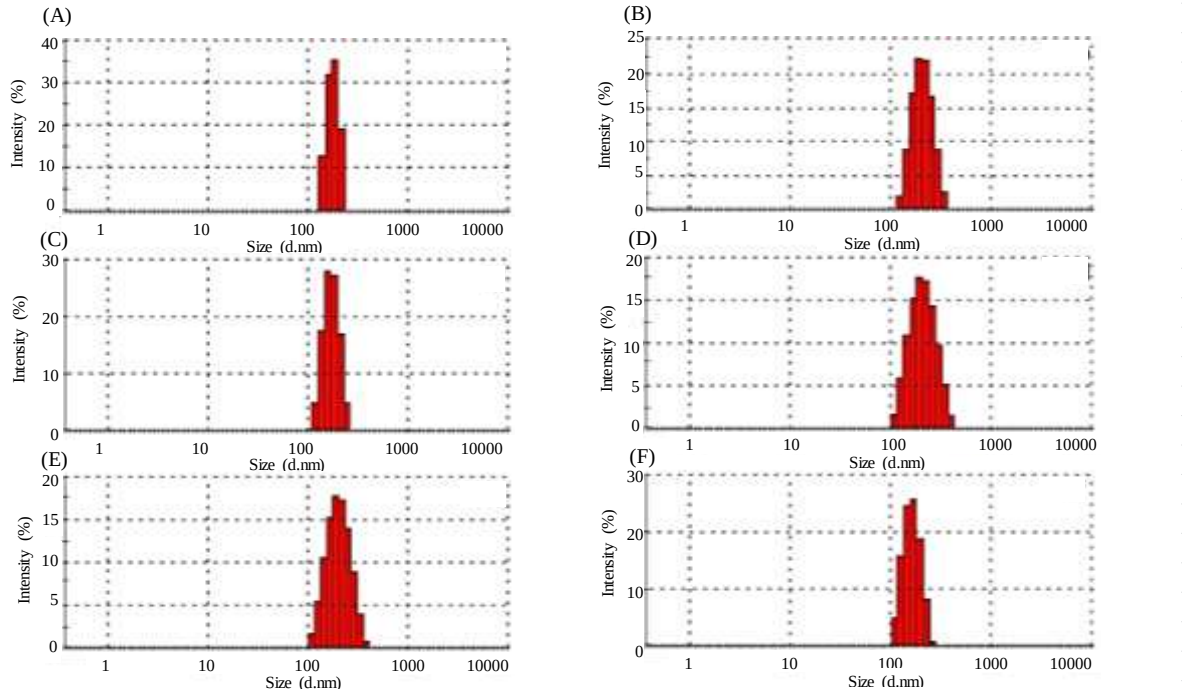

Figure 3 Particle size analysis obtained on parent $LiMn_2O_4$ and Co-doped $LiMn_2O_4$ such as (A) pure $LiMn_2O_4$, (B) $LiMn_{1.9}Co_{0.1}O_{4-\delta}$, (C) $LiMn_{1.8}Co_{0.2}O_{4-\delta}$, (D) $LiMn_{1.7}Co_{0.3}O_{4-\delta}$, (E) $LiMn_{1.6}Co_{0.4}O_{4-\delta}$, (F) $LiMn_{1.5}Co_{0.5}O_{4-\delta}$ nanoparticles prepared by combustion technique.

Table 2 Particle size data of $LiMn_{2-x}Co_xO_{4-\delta}$ nanoparticles.

Samples	Peak 1		Average particle size (nm)
	% Intensity	Diameter (nm)	
$LiMn_2O_4$	100	181.7	294.9
$LiMn_{1.9}Co_{0.1}O_{4-\delta}$	100	218.0	210.5
$LiMn_{1.8}Co_{0.2}O_{4-\delta}$	100	179.4	234.9
$LiMn_{1.7}Co_{0.3}O_{4-\delta}$	100	211.2	210.8
$LiMn_{1.6}Co_{0.4}O_{4-\delta}$	100	208.2	230.4
$LiMn_{1.5}Co_{0.5}O_{4-\delta}$	100	159.4	196.6

3.4 SEM studies

The SEM photographs of the Co-doped $LiMn_2O_4$ nanoparticles synthesized by combustion method are shown in Figure 4. It is obvious that all the samples distributed with small and big sized grains which are distributed randomly. With increase in the cobalt content, the grain size generally increases. As indicated in XRD data, the crystallite size values also were found to decrease with the enhancement of Co concentration. Hence, grain size data found in SEM is in line with the XRD data. Also, agglomeration is also visible in all the type of samples which may be due to calcination process [20]. The samples are found to be fluffy because of combustion of fuel during the preparation of samples. The SEM images of $LiMn_{2-x}Co_xO_{4-\delta}$ nanoparticles confirm the uniformity of phase formation the particle size of the particles.

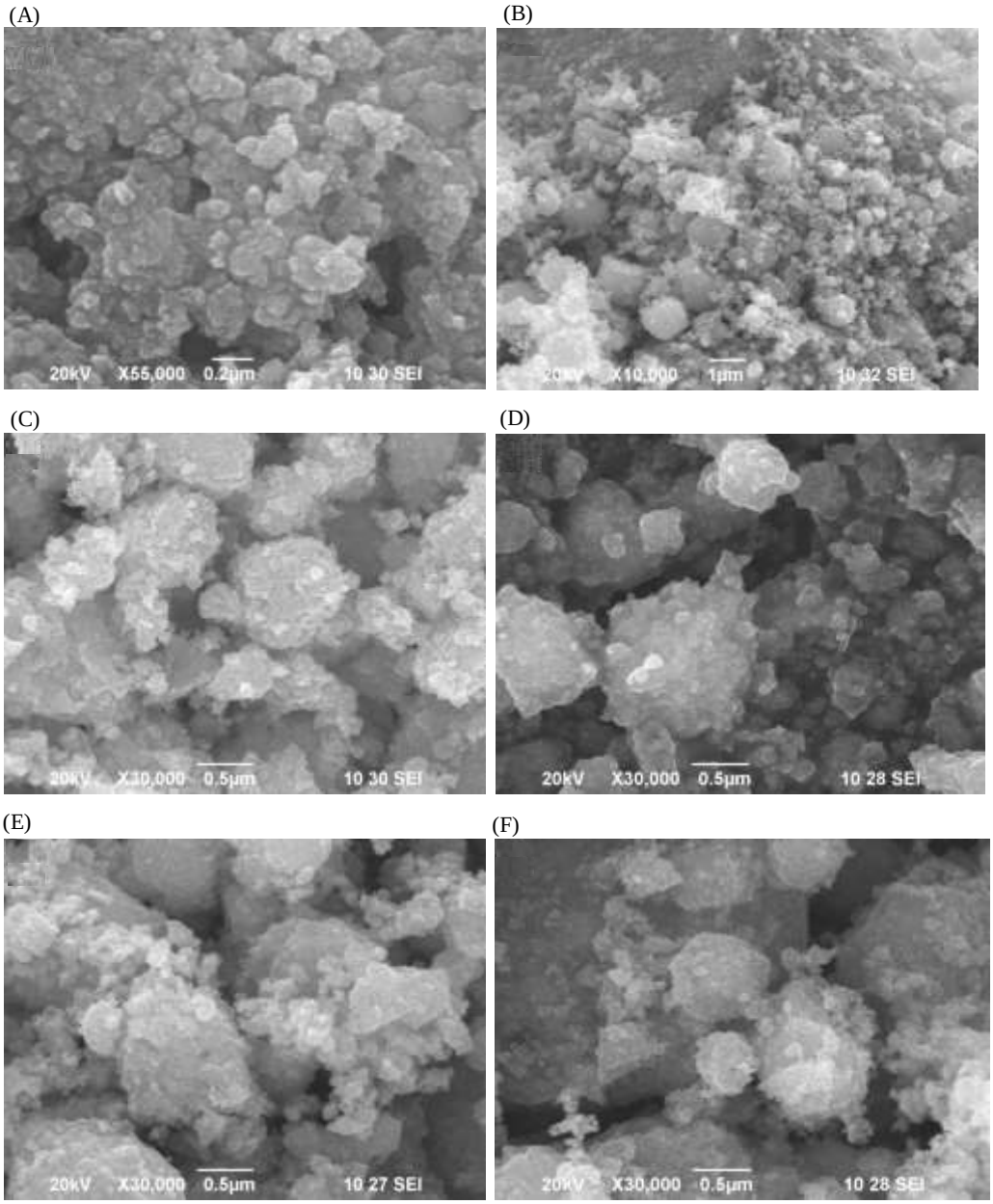

Figure 4 SEM photographs obtained on parent $LiMn_2O_4$ and Co-doped $LiMn_2O_4$ such as (A) pure $LiMn_2O_4$, (B) $LiMn_{1.9}Co_{0.1}O_{4-\delta}$, (C) $LiMn_{1.8}Co_{0.2}O_{4-\delta}$, (D) $LiMn_{1.7}Co_{0.3}O_{4-\delta}$, (E) $LiMn_{1.6}Co_{0.4}O_{4-\delta}$, (f) $LiMn_{1.5}Co_{0.5}O_{4-\delta}$ nanoparticles prepared by combustion technique.

3.5 EDAX studies

The chemical composition of $LiMn_{2-x}Co_xO_{4-\delta}$ nanoparticles were analyzed by Energy dispersive X-ray spectroscopy (EDAX). The EDAX patterns of the Co-doped $LiMn_2O_4$ nanomaterials prepared by combustion technique are shown in Figure 5. One can see the specific lines of Mn, Co, and O and not for any other impurity elements in the final products. It shows that no alteration of chemical composition due to calcination occur, that means preservation of crystalline structure and morphology as well, but of chemical composition, too. The EDAX data of elements present in nanocrystalline is given in Table 3. The data exhibited only the peaks relevant for Mn, Co and O atoms which again confirmed the absence any impurity atoms in the samples. Since Li has low energy radiation property, the atomic weight % of Li was not reflected in EDAX data.

(A)

(B)

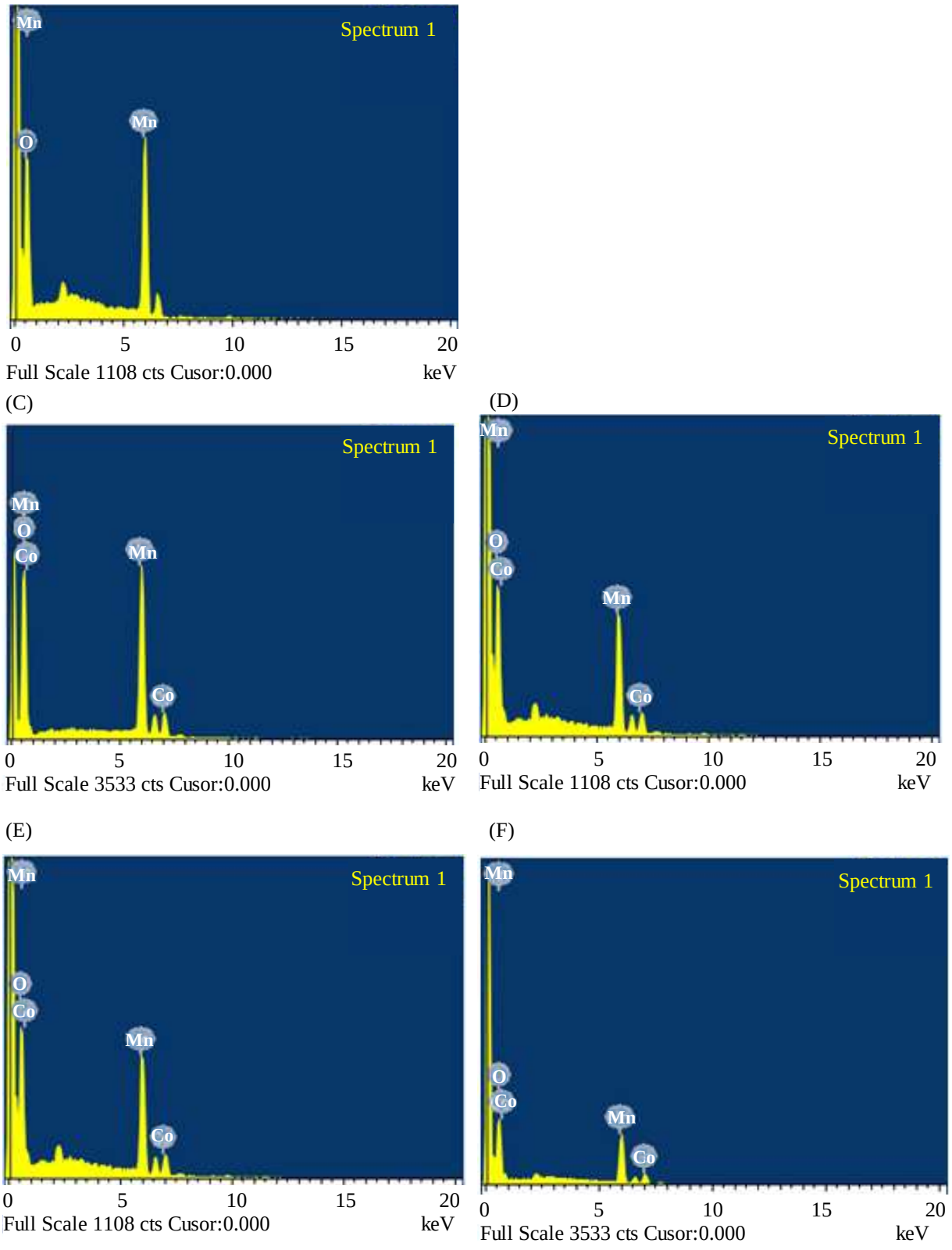

Figure 5 EDAX data obtained on nanocrystalline materials such as (a) pure $LiMn_2O_4$, (b) $LiMn_{1.9}Co_{0.1}O_{4-\delta}$, (c) $LiMn_{1.8}Co_{0.2}O_{4-\delta}$, (d) $LiMn_{1.7}Co_{0.3}O_{4-\delta}$, (e) $LiMn_{1.6}Co_{0.4}O_{4-\delta}$, (f) $LiMn_{1.5}Co_{0.5}O_{4-\delta}$ nanoparticles prepared by combustion technique.

Table 3 EDAX data obtained on $LiMn_{2-x}Co_xO_{4-\delta}$ nanoparticles**.**

Samples	Atomic weight % of elements		
	Mn	Co	O
$LiMn_2O_4$	31.61	--	68.39
$LiMn_{1.9}Co_{0.1}O_{4-\delta}$	29.65	2.34	68.00
$LiMn_{1.8}Co_{0.2}O_{4-\delta}$	28.12	3.75	68.13
$LiMn_{1.7}Co_{0.3}O_{4-\delta}$	21.07	3.84	75.09
$LiMn_{1.6}Co_{0.4}O_{4-\delta}$	24.05	5.27	70.69
$LiMn_{1.5}Co_{0.5}O_{4-\delta}$	20.76	6.89	72.35

3.6 Electrochemical impedance studies

Figure 6 displays the typical Nyquist ac impedance plots obtained on the cathode materials between the frequency ranges between 40 Hz to 1 MHz in the amplitude of 0.05 V at room temperature. The resulting Nyquist plots demonstrate an abnormal trend of the spinel materials. It is observed from the figure that the impedance spectra obtained for the entire samples shows depressed semicircle in the measured frequency range. The impedance spectrum is usually indicated as negative of imaginary part of impedance (-Z'') versus real part of impedance (Z'), which is referred as Nyquist plot. All the plots contain two semicircle arcs i.e., one semicircle at elevated frequency region and another semicircle tend to lesser frequency region. The semicircle shows the bulk and electrode phenomena, while that at intermediate frequencies symbolize the involvement of grain boundary. The presence of depressed semicircle exhibits the non-Debye character of the samples. Bulk resistance R_b was found out from the intercept of the semicircle at the low-frequency side of the plot with the real axis (Z') which improve the conductivity of $LiMn_2O_4$. It was reported that the semicircle at elevated frequency region can be ascribed to the electrolyte resistance and the surface film impedance and the semicircle at lesser frequency region can be ascribed to the lithium-intercalation process [32]. It was observed that the increase in the cobalt dopant levels in the $LiMn_2O_4$ lattice facilitates the enhancement of conductivity of the prepared samples. An equivalent circuit used to fit the impedance data using Zview software is given in figure. 7, which is similar to the circuit employed for the cathode of the lithium ion battery. In this circuit, R_1 indicates the resistance between the electrode and the current collecting material. The R_1 relates to the high frequency intercept at the real axis. R_2 is the resistance which is used to model another depressed semicircle. The first depressed semicircle (at the elevated frequency region) is ascribed to lithium ion diffusion through the passivation layer, and the second depressed semicircle (at the high-to-medium frequency region) is assigned to the charge transfer reaction of electrode material. The capacitance of double layer is represented by the capacitor (constant phase element, CPE). The electrical conductivity values for all the samples were calculated with the following equation [27] from the impedance spectra of the samples.

$$\sigma = d/R_bS \quad (3)$$

σ = Electrical conductivity in Scm^{-1}
d = Thickness of the sample in cm
S= Area of the sample in cm^2
R_b = Bulk resistance in ohm

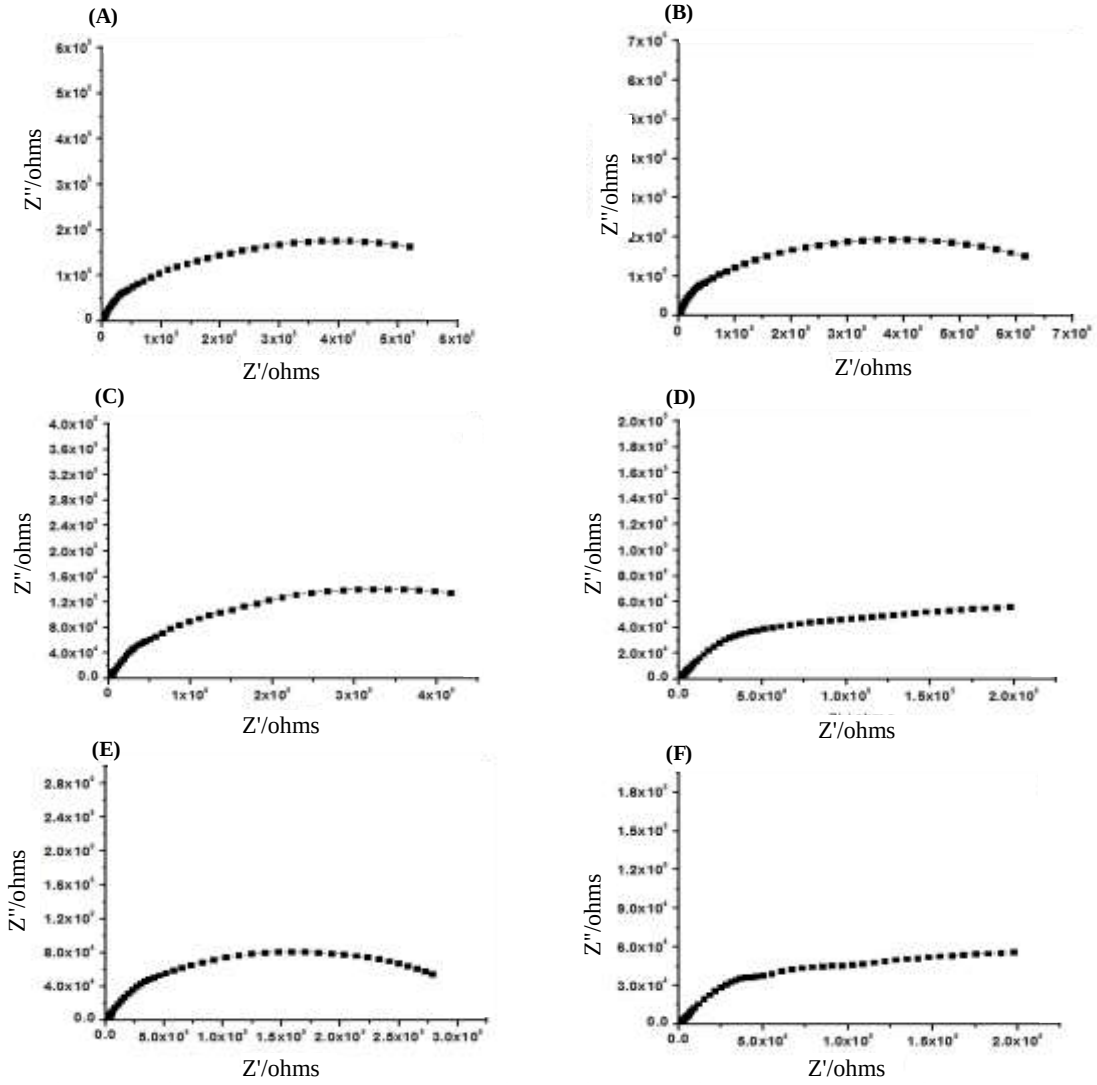

Figure 6 Electrochemical impedance spectra obtained on sintered cathode specimens (A) pure $LiMn_2O_4$, (B) $LiMn_{1.9}Co_{0.1}O_{4-\delta}$, (C) $LiMn_{1.8}Co_{0.2}O_{4-\delta}$, (D) $LiMn_{1.7}Co_{0.3}O_{4-\delta}$, (e) $LiMn_{1.6}Co_{0.4}O_{4-\delta}$, (f) $LiMn_{1.5}Co_{0.5}O_{4-\delta}$ at room temperature.

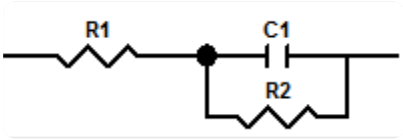

Figure 7 Equivalent circuit, used to fit measurement data obtained $LiMn_2O_4$ and Co-doped $LiMn_2O_4$ oxide pellets.

(Where, the symbol ⊣⊢ indicated for capacitor (constant phase element, CPE) and the symbol ⏦ used to represent the resistor)

Table 4 Conductivity values calculated for sintered $LiMn_2O_4$ and Co-doped $LiMn_2O_4$ using electrochemical impedance spectroscopy at room temperature (298 K).

Sample	Electrical conductivity (Scm^{-1})
$LiMn_2O_4$	1.58×10^{-6}
$LiMn_{1.9}Co_{0.1}O_{4-\delta}$	2.52×10^{-6}
$LiMn_{1.8}Co_{0.2}O_{4-\delta}$	3.22×10^{-6}
$LiMn_{1.7}Co_{0.3}O_{4-\delta}$	6.88×10^{-6}
$LiMn_{1.6}Co_{0.4}O_{4-\delta}$	7.66×10^{-6}
$LiMn_{1.5}Co_{0.5}O_{4-\delta}$	1.45×10^{-5}

The electrical conductivity values of the prepared spinel Co-doped $LiMn_2O_4$ samples calculated from the impedance plot and reported in the Table 4. From the Table 4, the intriguing phenomenon of the improved electrical transport was observed because of a highly conductive surface layer found in Co-doped $LiMn_2O_4$ pellet. The presence of surface-stabilized interstitial cations is postulated to explain the occurrence of a surface conduction. The diameter of the semicircle associates to the resistance of the grain. Such behaviour indicates a reduction in grain resistance of the samples and that the conduction process is activated with enhancement in the dopant (Co) concentration. Due to this, the enhancement of conductance was noticed for the samples having more Co dopant ion cocentration. Although these materials having moderate particle size, they tend to exhibit relatively good conductivity values owing to their special type of spinel structure and their promising surface characteristics. Among the samples studied, $LiMn_{1.5}Co_{0.5}O_{4-\delta}$ has shown better conductivity value (1.45×10^{-5} Scm^{-1}). All other samples have shown considerable conductivity values which make them as suitable alternative cathode components for Lithium-ion battery applications. The observed conductivity data is almost in line with the reported data (3.13×10^{-4} S cm^{-1} for $LiMn_2O_4$) [33]. Many research activities are being pursued by the researchers in $LiMn_2O_4$ based materials now-a-days [34-37].

4. Conclusion

Co-doped $LiMn_2O_4$ based cathode electrode samples were successfully prepared through one pot combustion method using urea as an organic fuel. The powder XRD data of the particles are well coordinated with the reported JCPDS data. XRD patterns have revealed the formation of well crystalline spinel structure. The XRD parameters were found in the range of 8.062-8.160 Å. FTIR results have shown the occurrence of M-O bond in all the samples with the peaks appeared at around 515.98 - 636.54 cm^{-1}. Particle size and SEM measurements have established the presence of nano-sized particles (196-294 nm) along-with few micron sized particles. The presence of atomic elements such as Mn, Co and O in the samples is confirmed by EDAX data. Since Li has low energy radiation property, the atomic weight % of Li was not reflected in EDAX data. From the room temperature conductivity measurements, it was found that $LiMn_{1.5}Co_{0.5}O_{4-\delta}$ sintered specimen has shown better conductivity value (1.45×10^{-5} Scm^{-1}) among all other samples studied. The electrochemical impedance studies confirmed that the samples doped with cobalt have smaller charge-transfer resistances and larger Li-ion diffusion coefficients than the parent spinel sample. From this, we propose that Co-doped $LiMn_2O_4$ may exhibit good electrochemical characteristics in real application for Li-ion batteries.

5. Acknowledgments

The authors AD and ASN thank Karunya Institute of Technology and Sciences (KITS) for promoting electrochemical energy conversion based research activity in the Department of Applied Chemistry. GS thanks University Grants Commission (UGC, Government of India) for providing Rajiv Gandhi Fellowship for Students with Disability (No. F./2013-14/RGNF-2013-14D-OBC-TAM-56465) to do his Ph.D. research work in the Department of Applied Chemistry, KITS.

6. References

[1] Nitta N, Wu FX, Lee JT, Yushin G. Li-ion battery materials: present and future. Materials Today 2015; 18:252-264.

[2] Armand M, Tarascon J M. Building better batteries. Nature 2008;451:652-657.

[3] Islam MS, Fisher CA. Lithium and sodium battery cathode materials: computational insights into voltage, diffusion and nanostructural properties. Chem Soc Rev. 2014;43(1):185-204.

[4] Tang YX, Zhang YY, Li WL, Ma B, Chen XD. Rational material design for ultrafast rechargeable lithium-ion batteries. Chem Soc Rev. 2015;44(17):5926-5940.

[5] Wu MQ, Zhang QY, Lu HP, Chen A. Nanocrystalline orthorhombic $LiMnO_2$ cathode materials synthesized by a two-step liquid-phase thermal process. Solid State Ion. 2004;169(1-4):47-50.

[6] Liu Q, Wang S, Tan H, Yang Z, Zeng J. Preparation and doping mode of doped $LiMn_2O_4$ for Li-ion batteries. Energies. 2013;6:1718-1730.

[7] Sahan H, Göktepe H, Dokan FK, Aydın A, Veziroglu S, Patat S. Improvement of cycling stability of $LiMn_2O_4$ cathode by Al_2O_3 surface coating for Li-ion batteries. Acta Physica Polonica A. 2013;123(2):368-370.

[8] Marchini F, Rubi D, Pozo M, Williams FJ, Calvo EJ. Surface chemistry and lithium-ion exchange in $LiMn_2O_4$ for the electrochemical selective extraction of LiCl from natural salt lake brines. J Phys Chem C. 2016;120(29):15875-15883.

[9] Xiao LF, Zhao YQ, Yang YY, Cao YL, Ai XP, Yang HX. Enhanced electrochemical stability of Al-doped $LiMn_2O_4$ synthesized by a polymer-pyrolysis method. Electrochimica Acta. 2008;54(2):545-550.

[10] Pugazhendhi A, Ellappan S, Kumaresan I, Paramasivam M. Dielectric and conduction mechanism studies of Ni doped $LiMn_2O_4$ synthesized by solution combustion method. Ionics. 2018;24:3745-3755.

[11] Song GM, Li WJ, Zhou Y. Synthesis of Mg-doped LiMn2O4 powders for lithium-ion batteries by rotary heating. Mater Chem Phys. 2004;87(1):162-167.

[12] Horata N, Hashizume T, Saiki A. Synthesis of Fe doped $LiMn_2O_4$ cathode materials for Li battery by solid state reaction. Arch Metell Mater. 2015;60:949-951.

[13] Piao JY, Duan SY, Lin XJ, Tao XS, Xu YS, Cao AM, et al. Surface Zn doped $LiMn_2O_4$ for an improved high temperature performance. ChemComme. 2018;54(42):5326-5329.

[14] Guoha L, Ikuta H, Uchida T, Wakihara M, The spinel phases $LiMyMn_2-yO4$ (M = Co, Cr, Ni) as the cathode for rechargeable lithium batteries. J Electrochem Soc. 1996;143:178-182.

[15] Shigang L, Zhenping C, Weihua J, Mingxun L, Songtao H. Preparation of modified $LiMn_2O_4$ by solid-state reaction. Rare Metals. 2006;25(6):71-76.

[16] Kiani MA, Mousavi MF, Rahmanifar MS. Synthesis of nano-and micro-particles of $LiMn_2O_4$: Electrochemical investigation and assessment as a cathode in Li battery. Int J Electrochem Sci. 2011;6(7):2581-2595.

[17] Naghash AR, Lee JY. Preparation of spinel lithium manganese oxide by aqueous co-precipitation. J Power Sources. 2000;85(2):284-293.

[18] Hui W, Lei JH, Chen YX, Sun YB, Yuan QH. The mechanism of sol-gel synthesis of normal spinel $LiMn_2O_4$ with chelation of citric acid. J Wuhan Univ Technol Mater Sci Ed. 2002;17(4):21-24.

[19] Zhu C, Nobuta A, Saito G, Nakatsugawa I, Akiyama T. Solution combustion synthesis of $LiMn_2O_4$ fine powders for lithium ion batteries. Adv Pow Metall. 2014;25(1):342-347.

[20] Stella KC, Nesaraj SA. Effect of fuels on the combustion synthesis of $NiAl_2O_4$ spinel particles. Iran J Mater Sci Eng. 2007;7(2):36-44.

[21] Tong QS, Yang Y, Shi JC, Yan JM, Zheng LG. Synthesis and storage performance of the doped $LiMn_2O_4$ spinel. J Electrochem Soc. 2007;154(7):A656-A667.

[22] Zhang LX, Wang YZ, Jiu HF, Wang YL, Sun YX, Li Z. Controllable synthesis of Co-doped spinel $LiMn_2O_4$ nanotubes as cathodes for Li-ion batteries. Electron Mater Lett. 2014;10:439-444.

[23] Li Q, Peng C, Huang J, Xu W, Yang F, Bai H, et al. Preparation and electrochemical properties of $LiMn_2O_4$ by solid-state combustion synthesis method using starch as a fuel. Int J Electrochem Sci. 2015;10:7513-7520.

[24] Singhal S, Chawla AK, Gupta HO, Chandra R. Influence of cobalt doping on the physical properties of Zn0.9Cd0.1S nanoparticles. Nanoscale Res Lett. 2010;5(2):323-331.

[25] Siqueira JM, Machado CT, Quattrociocchi DS, Garrido FS, Costa LM, Ponzio EA, et al. Experimental and theoretical study of $LiMn_2O_4$ synthesized by the solution combustion method using corn starch as fuel. J Braz Chem Soc. 2020;31(2):381-393.

[26] Chand P, Bansal V, Sukriti K, Singh V. Effect of pH values on structural, optical, electrical and electrochemical properties of spinel $LiMn_2O_4$ cathode materials. J Sci-Adv Mater Dev. 2019;4(2):245-251.

[27] León A, Reuque P, Garín C, Segura R, Vargas P, Zapata P, et al. FTIR and raman characterization of TiO2 nanoparticles coated with polyethylene glycol as carrier for 2-Methoxyestradiol. Appl Sci. 2017;7(1):49.

[28] Seyedahmadian M, Houshyarazar S, Amirshaghaghi A. Synthesis and characterization of nanosized of spinel $LiMn_2O_4$ via sol-gel and freeze drying methods. Bull Korean Chen Soc. 2013;34(2):622-628.

[29] Tas AC, Majewski PJ, Aldinger F. Chemical preparation of pure and strontium- and/or magnesium-doped lanthanum gallate powders. J Am Ceram Soc. 2000;83(12):2954-2960.

[30] Srikesh G, Nesaraj SA. Synthesis and characterization of phase pure NiO nanoparticles via the combustion route using different organic fuels for electrochemical capacitor applications. J Electrochem Sci Technol .2015;6(1):16-25.

[31] Campos EA, Pinto DS, Oliveira JI, Mattos EC, Dutra RC. Synthesis, characterization and applications of iron oxide nanoparticles - a short review. J Aerosp Technol Manag. 2015;7(3):267-276.

[32] Wang L, Zhao JS, He XM, Gao J, Li JJ, Wan CR, et al. Electrochemical impedance spectroscopy (EIS) study of LiNi1/3Co1/3Mn1/3O2 for Li-ion batteries. Int J Electrochem Sci. 2012;7(1):345-353.

[33] Rao BN, Padmaraj O, Narsimula D, Venkateswarlu M, Satyanarayana N. A.C conductivity and dielectric properties of spinel $LiMn_2O_4$ nanorods. Ceram Int. 2012;41(10 Pt 2):14070-14077.

[34] Yu Y, Junming G, Mingwu X, Changwei S, Xiaofang L, Hongli B, et al. Enhancing the durable performance of $LiMn_2O_4$ at high-rate and elevated temperature by nickel-magnesium dual doping. Sci Rep. 2019;9(1):16864. PMID:31728020.

[35] Liu QL, Wang SP, Tan H, Yang ZG, Zeng J. Preparation and doping mode of doped $LiMn_2O_4$ for Li-ion batteries. Energies. 2013;6(3):1718-1730.

[36] Wang SM, Liu HL, Xiang MW, Guo JM, Bai W, Bai H, et al. Improved electrochemical properties and kinetics of an LiMn2O4-based cathode co-modified via Cu doping with truncated octahedron morphology. New J Chem. 2020;2544:10569-10577.
[37] Abbas SM, Hashem AM, Ghany AE, Ismail EH, Kotlar M, Winter M, et al. Ag-modified LiMn2O4 cathode for lithium-ion batteries: coating functionalization. Energies. 2020;13(19):5194.